Title: *A Model for Simulating the Response of Aluminum Honeycomb Structure to Transverse Loading for* Proceedings of the **American Society for Composites – Twenty-Seventh Technical Conference**

Authors: James G. Ratcliffe[1]

Michael W. Czabaj[2]

Wade C. Jackson[2]

---

[1] National Institute of Aerospace, Hampton, VA Resident at Durability, Damage Tolerance, and Reliability Branch NASA Langley Research Center, Hampton, VA 23681

[2] Durability, Damage Tolerance, and Reliability Branch NASA Langley Research Center, Hampton, VA 23681

ABSTRACT

A 1-dimensional material model was developed for simulating the transverse (thickness-direction) loading and unloading response of aluminum honeycomb structure. The model was implemented as a user-defined material subroutine (UMAT) in the commercial finite element analysis code, ABAQUS®/Standard. The UMAT has been applied to analyses for simulating quasi-static indentation tests on aluminum honeycomb-based sandwich plates. Comparison of analysis results with data from these experiments shows overall good agreement. Specifically, analyses of quasi-static indentation tests yielded accurate global specimen responses. Predicted residual indentation was also in reasonable agreement with measured values. Overall, this simple model does not involve a significant computational burden, which makes it more tractable to simulate other damage mechanisms in the same analysis.

INTRODUCTION

Honeycomb structure consists of an array of repeating unit cells with a geometry such as the hexagonal shape illustrated in Figure 1 [1]. Cell wall thickness and cell size are typically varied, yielding honeycombs with a range of densities and out-of-plane properties aimed at serving a particular need. Honeycombs are manufactured out of a variety of materials, with aluminum and an aramid fiber paper, known as Nomex®[3] [2], being the most commonly utilized materials in aerospace applications. The relatively low density of honeycomb, combined with its high specific out-of-plane compression and shear properties, makes this type of structure well suited for weight-critical applications. For

---

[3] Nomex® is a registered trademark of E.I DuPont de Nemours, Wilmington, DE, USA.

example, sandwich structure consisting of honeycomb panels reinforced with stiff, thin facesheets, are often used in structural components of aerospace vehicles.

A drawback, however, of using honeycombs as core materials in sandwich structure is the propensity of the honeycomb to crush during a transverse loading event (such as low-velocity impact) [3-6]. This damage can result in a significant reduction of the in-plane compressive strength of the sandwich panel [3]. The problem is further exacerbated by the difficulty in detecting such damage, particularly after low-velocity impact events that may be barely visible. Consequently, some effort has been applied towards experimentally characterizing damage that arises from a low-velocity impact event and predicting the resulting residual in-plane compressive strength of the damaged panel [7-20]. In many of these examples, the simulations used to predict residual compressive strength involve an assumed initial damage state in the core material [10, 12, 14, 18] or completely disregard the effect of the core [11].

Researchers have also focused on predicting core damage in sandwich structures arising from localized, transverse loading [20-25]. Many of these efforts utilize beam theory solutions whereby a Winkler foundation is employed to represent the elastic response of the core material and plastic foundations to represent core crushing [21-22]. More recently [23-24], a modified beam theory analysis was conducted in which a beam is sectioned into segments allowing for the progressive development of indentation in the sandwich beam as transverse loading is applied. Finite element simulations have also been conducted for simulating low-velocity impact on sandwich structures [25]. In this example, dynamic analyses were performed, utilizing an elastic-perfectly plastic material parameter to represent thickness-direction loading of an aluminum honeycomb core. Other finite element simulations of honeycomb core-based sandwich structure [20] have been conducted where the cellular geometry of the core was explicitly modeled, and a plasticity model was utilized to capture yielding involved during the crush and post-crush response of the aluminum honeycomb. These models were applied to simulating the quasi-static indentation (QSI) on sandwich plates.

The vast majority of these simulations utilize an empirically based constitutive model for representing the response of honeycomb to transverse loading. These models are themselves based on data obtained from a flatwise compression/tension test (such as ASTM C365 [26]) of the honeycomb material in question. An adequate representation of this response is required in order to predict the extent of damage that arises in the honeycomb structure after a localized transverse loading event.

The objective of the work detailed in this paper was to develop a simple one-dimensional model for simulating the response of a honeycomb structure to transverse loading. As in previous cases, the model is based on the aforementioned constitutive relationship. However, the current effort differs from previous work because the model is implemented as a user material model into a commercial finite element analysis code (ABAQUS®[4]/Standard). Also, the parameters of the constitutive model can be easily modified by changing the user input of the material model. Finally, this simple approach does not involve a significant computational

---

burden, which makes it more tractable to simulate other damage mechanisms in the same analysis.

The remainder of this paper describes the development of the material model, its implementation into ABAQUS®/Standard, and the exercises undertaken to evaluate the material model.

CORE DAMAGE MATERIAL MODEL

The purpose of the model described in this section is to represent the response of aluminum honeycomb structure to transverse loading. The model is based on a transverse stress-strain relationship measured using a flatwise compression/tension test. This stress-strain relationship is implemented into ABAQUS®/Standard as a user-defined, 1-dimensional material model. Details of the model, its implementation into ABAQUS®/Standard and evaluation of the implemented model follow in the remainder of this section.

Constitutive Law

The stress-strain relationship on which the current honeycomb material model is based is typically measured using the flatwise-compression specimen depicted in Figure 2. The specimen is based on that detailed in the standard test methods for conducting flatwise compression and tension tests (ASTM C365 [26] and ASTM C297 [27], respectively), and consists of a 50mm-square block of honeycomb bonded between two loading blocks. A typical stress-strain response from a flatwise compression test is illustrated in Figure 3. Compressive loading is depicted by the solid grey lines in Figure 3, while the solid orange lines indicate unloading. Specimens are loaded in compression until the honeycomb cell walls begin to collapse, which generally corresponds to the sudden load drop shown in Figure 3. The honeycomb specimen continues crushing upon further compressive loading, which is characterized either by a stress plateau or a slight increase in stress as indicated in Figure 3. The specimen is unloaded after the required amount of core crushing has been obtained. This initially results in an elastic response from the specimen as the collapsed cell walls begin to deform. At some point during unloading, the specimen undergoes an overall reduction in stiffness, which is attributed to plastic deformation in aluminum honeycombs [23]. Complete unloading of the specimen either involves fracturing of the cell walls [23], or further plastic deformation, resulting in a residual tensile stress [20] as depicted in Figure 3. This constitutive relationship is specific to aluminum honeycombs and so may well adopt a different form in honeycombs made from other materials.

The current model idealizes the stress-strain relationship in Figure 3 as a series of linear functions depicted by the dashed lines in the figure. The parameters associated with this idealization are also depicted in the figure and act as the user input for the implementation of this model into ABAQUS®/Standard.

Implementation of Model into ABAQUS®/Standard

The constitutive model described in the previous section and illustrated in Figure 3 is implemented into ABAQUS®/Standard as a user material model (UMAT) [28]. The implemented model can be used with 2-node truss elements (ABAQUS®/Standard element type T3D2) in a finite element analysis in which the truss elements are used to represent a honeycomb structure. The UMAT is in the form of a user-defined subroutine, written in the computer language, FORTRAN 77. ABAQUS®/Standard provides the user with access to a range of its own subroutines that may be called within the UMAT, enabling access to information such as analysis variables (state, field, etc.) and analysis time (step and increment number, time step, etc.). The parameters that define the constitutive model (Figure 3) are provided by the user in the analysis job input file (.inp) that contains all other user-defined information (node numbering, mesh connectivity, material, properties, load and boundary conditions, etc.) necessary for running an analysis. The UMAT is called at the time of executing an analysis at which point the UMAT is compiled and configured for operation within the analysis job. Operation of the UMAT within a finite element analysis proceeds as follows:

1. Analysis begins and user-input (Figure 3) is read by the UMAT.
2. The UMAT computes the tangent moduli, E_1, E_2, and E_3, (Figure 3).
3. At the beginning of each analysis increment, the current strain and strain increment is provided to the UMAT by ABAQUS®. The UMAT checks these values against the strain values that define key stages of deformation in the constitutive model (e_1, e_2, and e_3 in Figure 3). The strain increment is used to determine the direction of loading in an element.
4. The UMAT checks the current compressive strain value against a previously stored maximum value. If the current value exceeds the stored value then this strain is replaced by the current strain. For instance, if the current strain is -1010$\mu\varepsilon$ and the stored value is -1000$\mu\varepsilon$ then the stored value is replaced by the value of the current strain. This information is used to store the current damage state in an element.
5. A tangent modulus is selected based on the current strain and strain increment. This modulus is assigned to the stiffness matrix of the element. The stress in the element is then computed using the selected tangent modulus and the current strain increment.
6. The tangent stiffness and stress values are reported to ABAQUS®.
7. Steps 5 and 6 are repeated until the analysis converges corresponding to the end of the increment.
8. Steps 3-7 are repeated until completion of an analysis step(s).

The above operation is performed for each truss finite element. Additionally, a state of damage is defined in each element that corresponds to one of the three damage states depicted in Figure 3 (numbers in parenthesis in Figure 3). Damage state 1 corresponds to the region of the constitutive model before cell wall collapse has occurred (i.e. the initial elastic response). Damage state 2 corresponds to the region of the constitutive model during initial cell wall collapse. Damage state 3 corresponds to the region of the constitutive model during continued crushing of the

honeycomb. This information is used by the UMAT to determine the correct tangent stiffness during unloading (as illustrated by the dashed arrows in Figure 3) and also to provide a record of the damage state of each element at any moment during an analysis.

Evaluation of Material Model

SIMULATION OF QSI TESTS

The UMAT was evaluated by applying it to finite element analyses of a sandwich plate subjected to quasi-static indentation (QSI) loading. This test case was chosen because the specimen response does not involve flexure, which would not be captured by the current one-dimensional model. The sandwich plate consisted of an aluminum honeycomb core reinforced with quasi-isotropic graphite/epoxy composite facesheets. Complete details of the sandwich plate are given in Figure 4. QSI tests were previously conducted on this sandwich plate using a 25mm-diameter indenter and also a 76mm-diameter indenter [19]. Specimens were supported by a rigid back plate during each QSI test. A schematic of the test configuration is shown in Figure 4. The indentation/force response of each specimen was recorded in addition to the residual indentation in the sandwich plate at the end of each test [19]. Finite element analyses of these two test cases were conducted as part of an exercise to evaluate the developed UMAT. The 76mm indenter test case was deemed appropriate for evaluating the UMAT because the QSI response of the specimens was found to be largely attributed to core damage rather than facesheet damage [19], which is not accounted for in the following analyses. Even though significant facesheet damage (in the form of delamination) was observed in the 25mm indenter case, an analysis of this case was conducted nonetheless. In both cases, static, geometrically nonlinear analyses were conducted in order to account for indenter contact (as described below).

Finite element models used in the current evaluation of the UMAT consisted of 4-node shell elements (ABAQUS® type S4) to represent the upper facesheet. Each node of the shell elements was connected to 2-node truss elements, (ABAQUS® type T3D2) used to represent the honeycomb core. The length of the truss elements was equal to the honeycomb core height (in this case 25mm). A typical finite element mesh is shown in Figure 5 (only small number of truss elements are illustrated in the figure for clarity). Two-axis symmetry was assumed in the analysis in order to reduce the overall model size. Therefore, the center of the sandwich specimen corresponds to the corner of the mesh labeled 'A' in Figure 5. A relatively fine mesh was used to represent the facesheet with an element length of 0.5mm. All shell elements representing the facesheet had 1:1 aspect ratios. A similar meshing scheme was shown to yield a converged solution in a similar analysis conducted previously [18], and therefore a mesh convergence study was deemed to be unnecessary in the current case. The facesheet that made contact with the rigid back plate in actual tests (as illustrated in Figure 4) was initially modeled with shell elements. However, this was found to be unnecessary and instead the boundary condition detailed in Figure 5 (w=0) was used to represent the supported specimen side. The stacking sequence of the upper facesheet was represented using a composite stack feature provided by ABAQUS®/Standard, where the ply

orientation corresponded to the coordinate system shown in Figure 5. The nine engineering constants used to define the elastic response of the facesheet plies (facesheet damage was not considered in the current analyses) are presented in TABLE I, which also includes user input for the UMAT. The UMAT input data were obtained from previous flatwise compression/tension tests conducted on the sandwich structure in question [20]. The spherical indenters were represented using rigid elements (ABAQUS®/Standard type R3D3 and R3D4) and a frictionless contact algorithm provided by ABAQUS® was employed to facilitate contact between the rigid indenter elements and the shell elements representing the upper facesheet. The indenter mesh was positioned such that the node corresponding to the indenter tip was coincident with the plane of the facesheet, and the in-plane position of the indenter tip corresponded to the center of the sandwich specimen. Loading was applied to the rigid indenter mesh by prescribing a displacement along the global z-axis to a reference node positioned in the center of the indenter as shown in Figure 5. The nodes of the rigid indenter mesh were kinematically coupled with this dummy node such that they mimic any translation and rotation prescribed at this node. All prescribed boundary conditions are illustrated in Figure 5. Two analyses were performed for simulating QSI tests conducted using a 25mm-diameter and 76mm-diameter indenter, respectively. Each analysis was conducted in two steps. The first step involved translating the indenter in the z-axis towards the specimen up to a maximum prescribed indentation (denoted as z_{max} in Figure 5). In the second step, the prescribed indenter translation was reversed until the indenter returned to its position. The maximum allowed time over which a solution is sought during an increment (referred to as 'time increment' in ABAQUS® terminology), $\Delta t_{inc-max}$, was limited to 0.1% of the total time step in each analysis (this limit on $\Delta t_{inc-max}$ was imposed as a result of the study described at the end of this section). The computed indentation/force response and residual indentation profiles from both analyses were compared with corresponding data measured previously [19].

MAXIMUM ANALYSIS TIME INCREMENT

A static, geometrically nonlinear analysis in ABAQUS® is comprised of a series of steps such as those detailed above for translating the rigid indenter. In turn, each step is partitioned into a number of increments for which ABAQUS® attempts to converge to a solution. Typically, the amount of time step over which ABAQUS® attempts to converge to a solution, otherwise known as the time increment, is set to a relatively small value at the beginning of an analysis step. As the analysis proceeds, and if convergence is easily found, ABAQUS® automatically increases the time increment up to a maximum time increment that is either set by the user or ABAQUS® (see [29] for further details on analysis solution strategies utilized by ABAQUS®). It was found that the solution of an analysis utilizing the currently developed UMAT was very sensitive to this maximum time increment, $\Delta t_{inc-max}$. This sensitivity was investigated using the analysis of the QSI test involving the 76mm-diameter indenter. During this study, an analysis of this test configuration was repeated five times, each using a different value of $\Delta t_{inc-max}$, ranging from 2% of the total time step to 0.1% of the total time step (in each case, the initial time increment was kept constant at 0.1% of the total

time step). The indentation/force responses and residual indentation profiles were computed and checked for convergence relative to $\Delta t_{inc-max}$.

RESULTS / DISCUSSION

Simulation of QSI Tests

The compressive force/indentation responses computed from simulations of the QSI tests with a 25mm-diameter indenter and 76mm-diameter indenter are presented in Figure 6. The indentation/force response from the actual tests is superimposed onto each plot. The overall force/indentation response is captured very well by comparison to the measured responses. The beginning of each response is linear, corresponding to the initial linear response of the honeycomb. After some point, the honeycomb cell walls begin collapsing, which is characterized by an initial reduction in overall stiffness of the specimen (stiffness here is defined as the gradient to the tangent of the indentation/force curve). The amount of crushed honeycomb increases as indentation is increased. However, this is accompanied by an increase in contact area of the indenter with the neighboring facesheet. Consequently, continued indentation results in a gradual increase in specimen stiffness. After the maximum indentation is reached the indenter is returned to its original position. The resulting unloading is nonlinear largely because the amount of contact area between the indenter and specimen reduces upon further unloading.

The computed residual indentation profiles (along Segment AB in Figure 5) from analyses of the 25mm-diameter and 76mm-diameter indenter cases are presented in Figure 7. The computed dent profiles are mirrored about the yz plane (Figure 5) in order to provide a meaningful comparison with the measured dent profiles. The measured residual indentation profiles [19] are superimposed onto both plots for comparison. The results show that the analysis of the 25mm indenter case overestimated the residual indentation area although the correct overall shape of the dent, including the maximum indentation, was reproduced. The computed residual indentation from analysis of the 76mm indenter case was very close to the measured dent profile.

The peak applied force, residual indentation and total energy dissipation (area encompassed by the force/indentation responses) computed from both analyses are presented in TABLE II. The corresponding measured values are also included in the table for comparison. In the 25mm-diameter indenter case, the computed peak force is almost identical to the measured value (less than 1% difference). The computed residual indentation for this case, however, underestimates the measured value by almost 19%. The computed total energy dissipation compares more favorably and underestimated the measured value by 10%. This significant difference in dent profiles is likely attributed to the fact that significant delamination was observed in the 25mm indenter case, which was not accounted for in the current analysis.

The peak force computed from the analysis of the 76mm-diameter indenter case was again in excellent agreement with the measured value (less than 1% difference). The computed residual indentation was in better agreement with the

measured value (compared to the 25mm-diameter indenter case) and in this case underestimated the measured residual indentation by only 6%. The computed total energy dissipation underestimated the measured value by just under 10%. This relatively improved agreement in the 76mm indenter case is consistent with the fact that the specimen response was largely attributed to core damage [19].

In general, the overall computed specimen response compares very favorably with the experimental data in the 76mm indenter case, and suggests that the implemented one-dimensional material model is successful in capturing the response of honeycomb structure to transverse loading.

Maximum Analysis Time Increment

The maximum allowed time step during each increment, $\Delta t_{inc-max}$, in the above two analyses was limited to 0.1% of total time step. As mentioned previously, this limit was imposed as a result of a study conducted to determine the effect of maximum allowed time step on analysis results. The results of this study (based on analyses of the 76mm-diameter indenter case) are presented in Figure 8, where the computed peak force (Figure 8a) and maximum residual indentation (Figure 8b) are plotted as functions of the number of increments per analysis step. The number of increments per step is the reciprocal of $\Delta t_{inc-max}$, and the results are plotted in this manner to highlight the convergence of the solutions. Included in the plots are the measured peak force and residual indentation for this test case (denoted by dashed horizontal lines in each plot). Both plots show that the computed values tend to converge towards their measured counterparts as the number of increments per analysis step increases. Hence, from these results it was assumed that a converged solution was obtained when the number of increments per step was greater than or equal to 1000, i.e. when $\Delta t_{inc-max}$ 0.001.

SUMMARY AND CONCLUDING REMARKS

A material model for representing transverse loading of honeycomb structure was implemented as a material model into the commercial finite element analysis code, ABAQUS®/Standard. The model is based on an empirically determined stress-strain relationship measured using a flatwise/compression specimen. The exercises conducted for evaluating the UMAT resulted in the following general observations:

- The results from analyses of the quasi-static indentation (QSI) tests showed overall good agreement with the corresponding test data. This favorable comparison indicates that the one-dimensional material model can adequately capture the honeycomb core response, at least for QSI simulations.
- Results from analyses that employ the implemented material model would be sensitive to the time step taken during each analysis increment. However, this study indicated that a converged solution could be found when the maximum time increment in an analysis step was limited to 0.1% of the total time step.

- In general, this simple approach does not involve a significant computational burden, which should make it more tractable to simulate other damage mechanisms in the same analysis

REFERENCES

1. Hexcel Corporation, 2007. "Hexweb® Honeycomb Attributes and Properties"
2. Flame Resistant Nomex®. 2012. DuPont.10 July. 2012
   <http://www.easybib.com/reference/guide/mla/website>.
3. Cvitkovich, M.K., and W. C. Jackson. 1999. "Compressive Failure Mechanisms in Composite Sandwich Structures," *Journal of the American Helicopter Society*, 44(4):260-268.
4. Kim, C. G. and E. Jun. 1992. "Impact Resistance of Composite Laminated Sandwich Plates," *Journal of Composite Materials*, 26:2247-2261.
5. Zhou, G., M. Hill, J. Loughlan, and N. Hookham. 2006. "Damage Characteristics of Composite Honeycomb Sandwich Panels in Bending Under Quasi-Static Loading," *Journal of Sandwich Structures and Materials*, 8(1):55-90.
6. Abrate, S. 1997. "Localized Impact on Sandwich Structures with Laminated Facings," *Applied Mechanics Review*, 50(2):69-82.
7. Toribio, M.G., J. M. Marizo, and M. S. Spearing. "Compressive Failure of Notched Composite-Honeycomb Sandwich Panels," Presented at the 12th International Conference on Composite Materials, Paris, 1999.
8. Marizo, J.M. and M. S. Spearing. 2001. "Damage Modeling of Notched Graphite/Epoxy Sandwich Panels in Compression," *Applied Composite Materials*, 8(3):91-216.
9. Toribio, M.G. and M. S. Spearing. 2001. "Compressive Response of Notched Glass-Fiber Epoxy/Honeycomb sandwich Panels," *Composites: Part A*, 32:859-870.
10. Kassapoglou, C., 1996. "Compression Strength of Composite Sandwich Structures After Barely Visible Impact Damage," *ASTM Journal of Composites Technology and Research*, 18(4):274-284.
11. Ratcliffe J., W. C. Jackson, and J. Schaff. "Compression Strength Prediction of Impact-Damaged Composite Sandwich Panels," Presented at the American Helicopter Society 60th Annual Forum, Baltimore, MD, June 7-10, 2004.
12. Minguet, P.J., "A Model for Predicting the Behavior of Impact-Damaged Minimum Gage Sandwich Panels Under Compression," Presented at the AIAA/ASME/ASCE/AHS/ASC 32nd Structures, Structural Dynamics, and Materials Conference, Paper AIAA-91-1075-CP, 1991.
13. Tsang, P. H. W., "Impact Resistance and Damage Tolerance of Composite Sandwich Panels," Ph.D. dissertation, Massachusetts Institute of Technology, June 1994.
14. Moody, R. C. and A. J. Vizzini. "Incorporation of a Compliance Change Due to Impact in the Prediction of Damage Growth in Sandwich Panels," Presented at the 13th International Conference on Composite Materials, Beijing, China, June 2001.
15. Tsang, P. H. W. and P. Lagace. "Failure Mechanisms of Impact-Damaged Sandwich Panels Under Uniaxial Compression," Presented at the AIAA/ASME/ASCE/AHS/ASC 35th Structures, Structural Dynamics, and Materials Conference, Paper AIAA-94-1396-CP, 1994.
16. Moody, R. C., and A. J. Vizzini. "Test and Analysis of Composite Sandwich Panels with Impact Damage," DOT/FAA/AR-01/124, U.S. Department of Transportation, Federal Aviation Administration, March 2002.
17. Xie, Z., and A. J. Vizzini. 2005. "Damage Propagation in a Composite Sandwich Panel Subjected to Increasing Uniaxial Compression after Low-velocity Impact," *Journal of Sandwich Structures and Materials*, 7(4):269- 288.
18. Ratcliffe, J. and W. C Jackson. "A Finite Element Analysis for Predicting the Residual Compressive Strength of Impact-Damaged Sandwich Panels," NASA Technical Memorandum, NASA/TM-2008-215341, August 2008.
19. Singh, A. K., B. D. Davidson, D. P. Eisenberg, M. W. Czabaj, and A. T. Zehnder. 2012. "Damage Characterization of Quasi-Statically Indented Composite Sandwich Structures," *Journal of Composite Materials*, doi: 10.1177/0021998312446500.

20. Czabaj, M. W., "Damage and Damage Tolerance of High Temperature Composites and Sandwich Composite Structures," Ph.D. dissertation, Cornell University, August 2010.
21. Zenkert, D., A. Shipsha, and K. Persson. 2004. "Static Indentation and Unloading Response of Sandwich Beams,"*Composites Part B*, 35(6-8):511-522.
22. Shuaeib, F. M. and P. D. Soden. 1997. "Indentation Failure of Composite Sandwich Beams," *Composites Science and Technology*, 57(9-10):1249-1259.
23. Minakuchi, S., Y. Okabe, and N Takeda. 2008. "Segment-Wise Model for Theoretical Simulation of Barely Visible Indentation Damage in Composite Sandwich Beams: Part I - Formulation," *Composites Part A*, 39(1):133-144.
24. Minakuchi, S., Y. Okabe, and N Takeda. 2007. "Segment-Wise Model for Theoretical Simulation of Barely Visible Indentation Damage in Composite Sandwich Beams: Part II – Experimental Verification and Discussion," *Composites Part A*, 38(12):2443-2450.
25. Besant, T., G. A. O. Davies, and D. Hitchings. 2001. "Finite Element Modelling of Low Velocity Impact of Composite Sandwich Panels," *Composites Part A*, 32(9):1189-1196.
26. ASTM C365/C365M-05 "Standard Test Method for Flatwise Compressive Properties of Sandwich Cores," 2008 Annual Book of ASTM Standards, Vol.15.03.
27. ASTM C3297/C297M-04 "Standard Test Method for Flatwise Tensile Strength of Sandwich Constructions," 2008 Annual Book of ASTM Standards, Vol.15.03.
28. ABAQUS® 6.11 User Subroutines Reference Manual, Simulia, 2011.
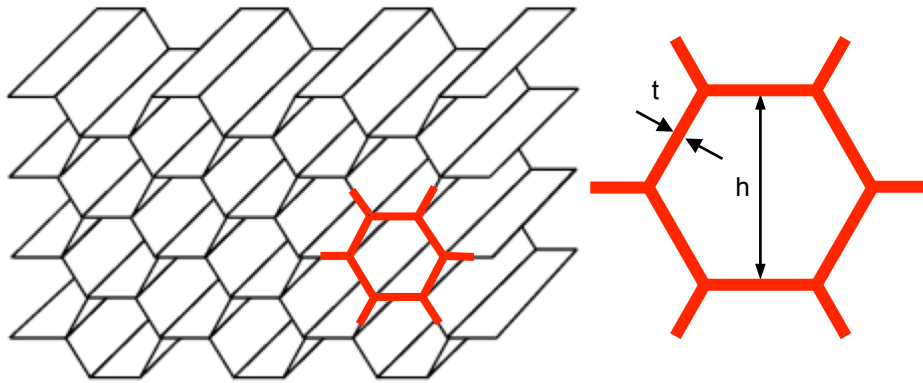29. ABAQUS® 6.11 Analysis User's Manual, Simulia, 2011.

Figure 1. Hexagonal cell geometry of a honeycomb structure.
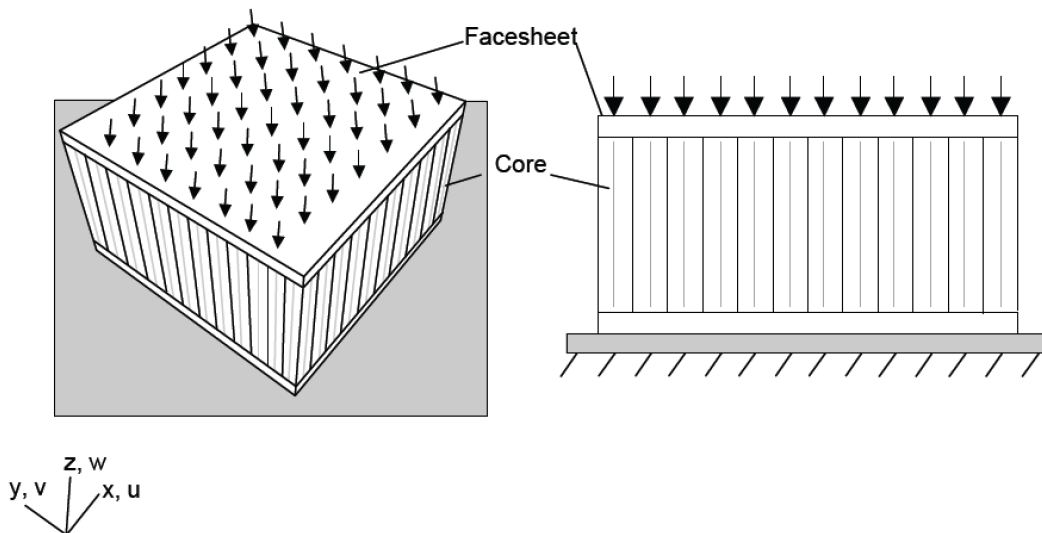

z, w
y, v   **x, u**

Figure 2. Schematic of a 50mm-square flatwise compression specimen.
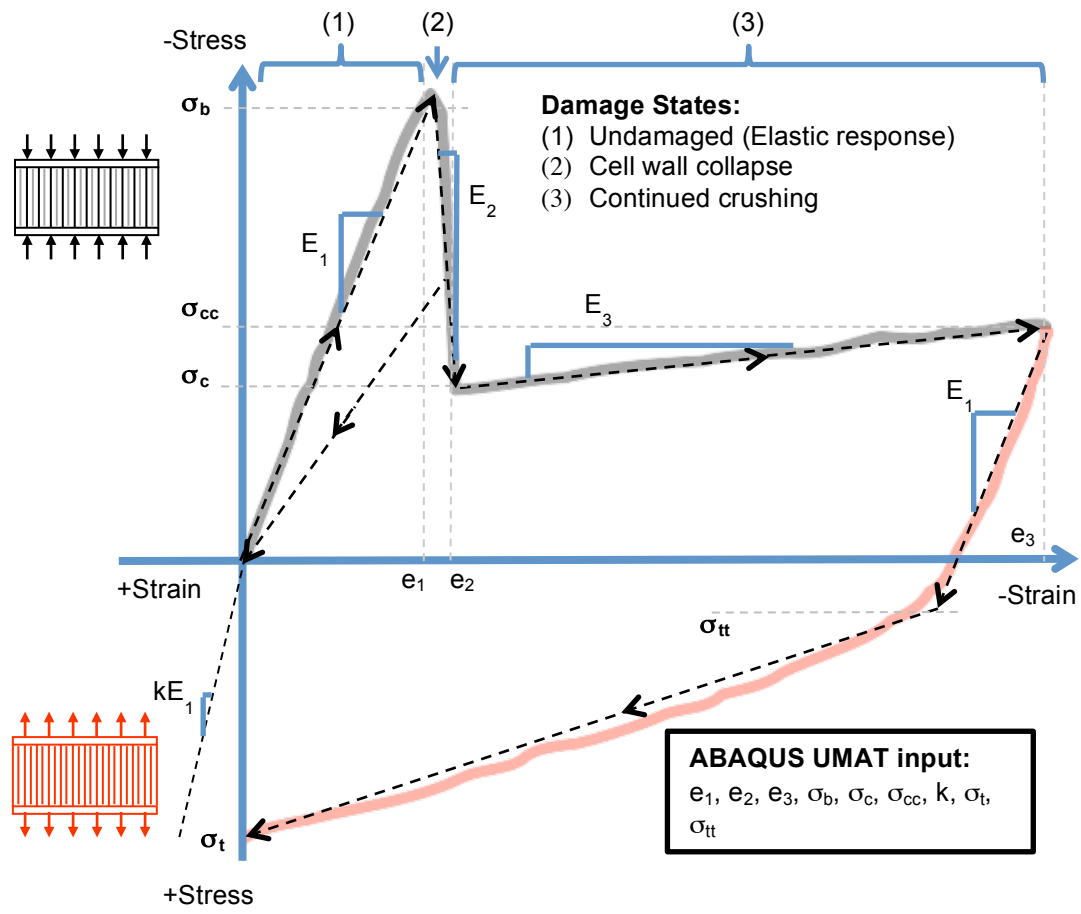
Figure 3. Idealized stress-strain relationship of honeycomb structure.

Sandwich plate details:

Facesheets:
8-ply graphite/epoxy tape
Layup [45/0/-45/90]$_2$
Thickness: 1.02mm
Core:
Aluminum (5052) honeycomb
Density: 50kg/m^3
Cell size: 3.2mm
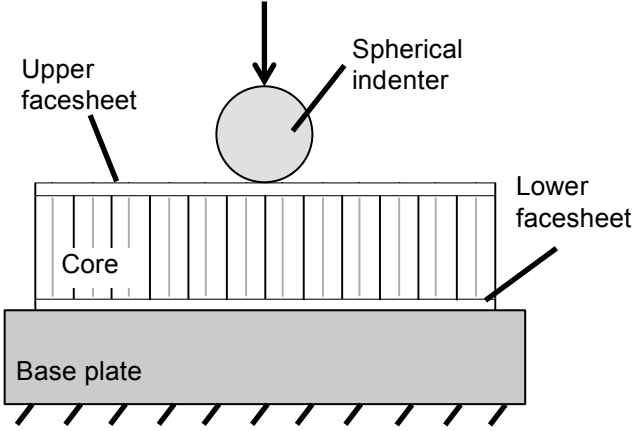Cell wall thickness: 0.02mm
Height: 25.4mm
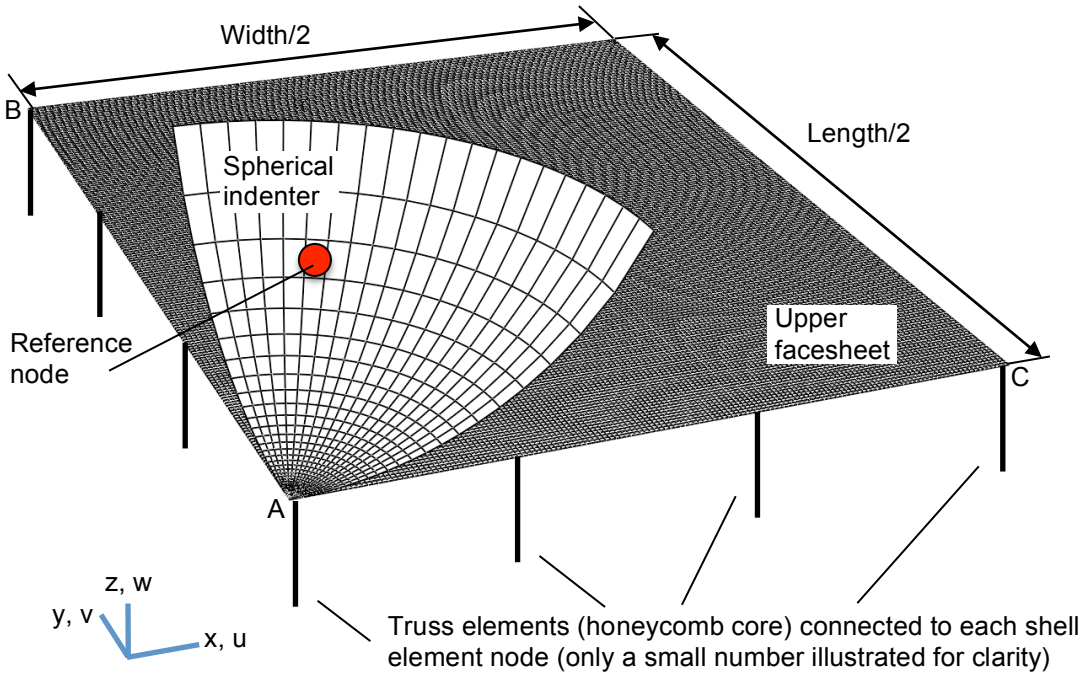**Sandwich plate dimensions:**
Width: 152mm
Length: 178mm

Spherical indenter

Upper facesheet

Lower facesheet

Core

Base plate

Figure 4. Details of quasi-static indentation test setup [20].

Width/2

Length/2

B

Spherical indenter

Reference node

Upper facesheet

C

A

z, w

y, v

x, u

Truss elements (honeycomb core) connected to each shell element node (only a small number illustrated for clarity)

BOUNDARY CONDITIONS:

Nodes along Segment AB:
$u=0$; $\phi_y=0$*
Nodes along Segment AC:
$v=0$; $\phi_x=0$*
Truss nodes (side opposite facesheet):
$w=0$

Reference node:
Fixed except for $w=z_{max}$
$z_{max}=1.44$mm (25mm indenter case)
$z_{max}=2.57$mm (76mm indenter case)

* ϕ_i denotes rotation about the ith axis

Figure 5. Finite element mesh and boundary conditions of QSI analyses (76mm indentor shown).
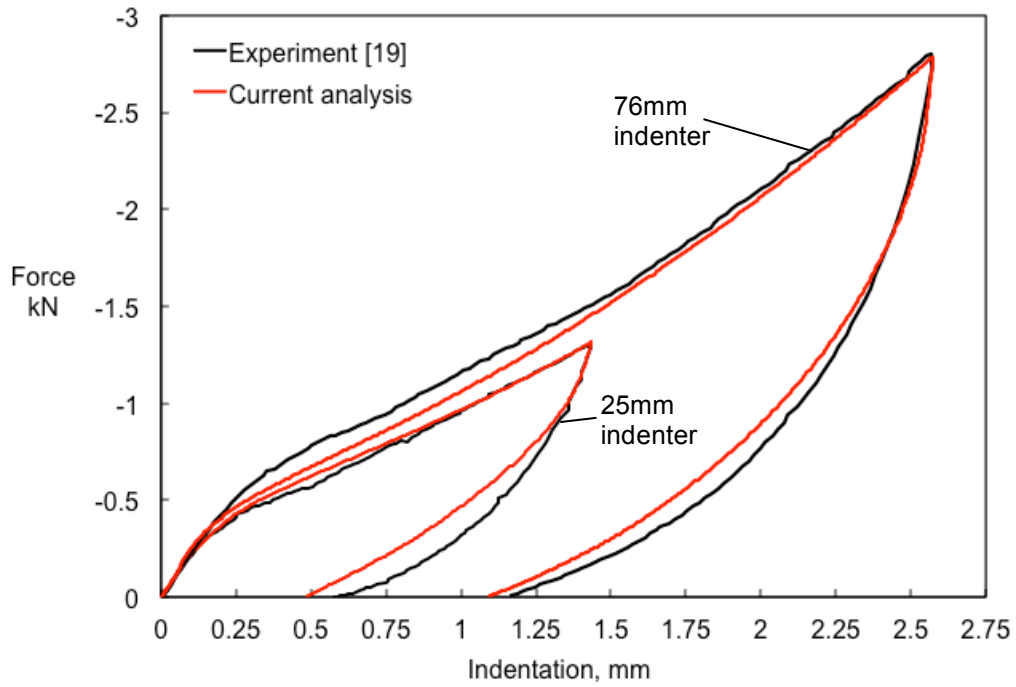
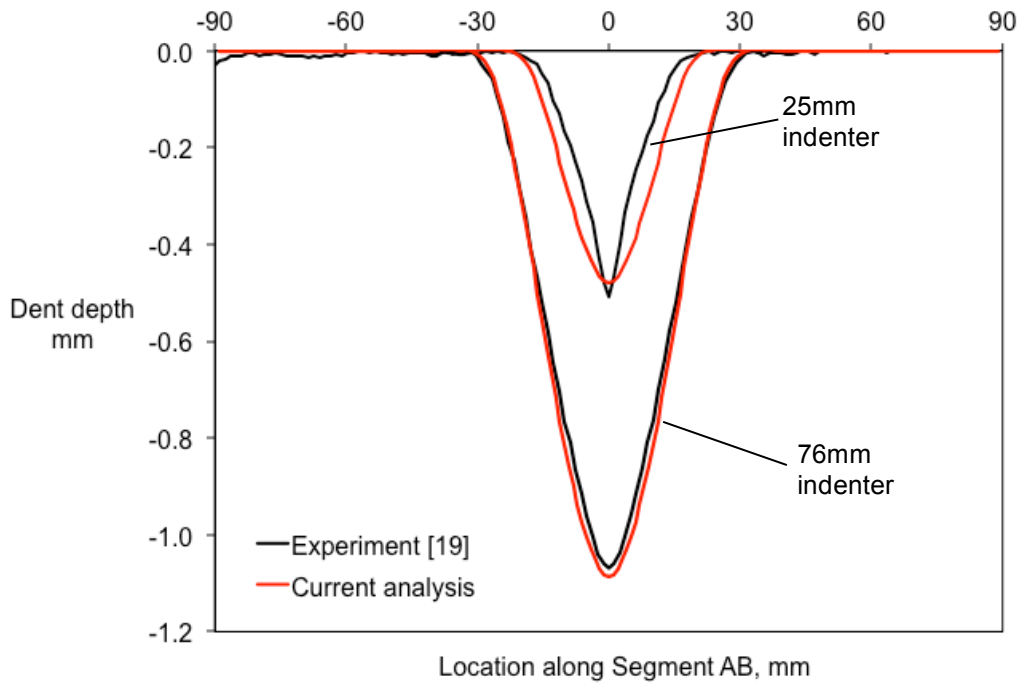Figure 6. Computed versus measure force/indentation response of QSI specimens.

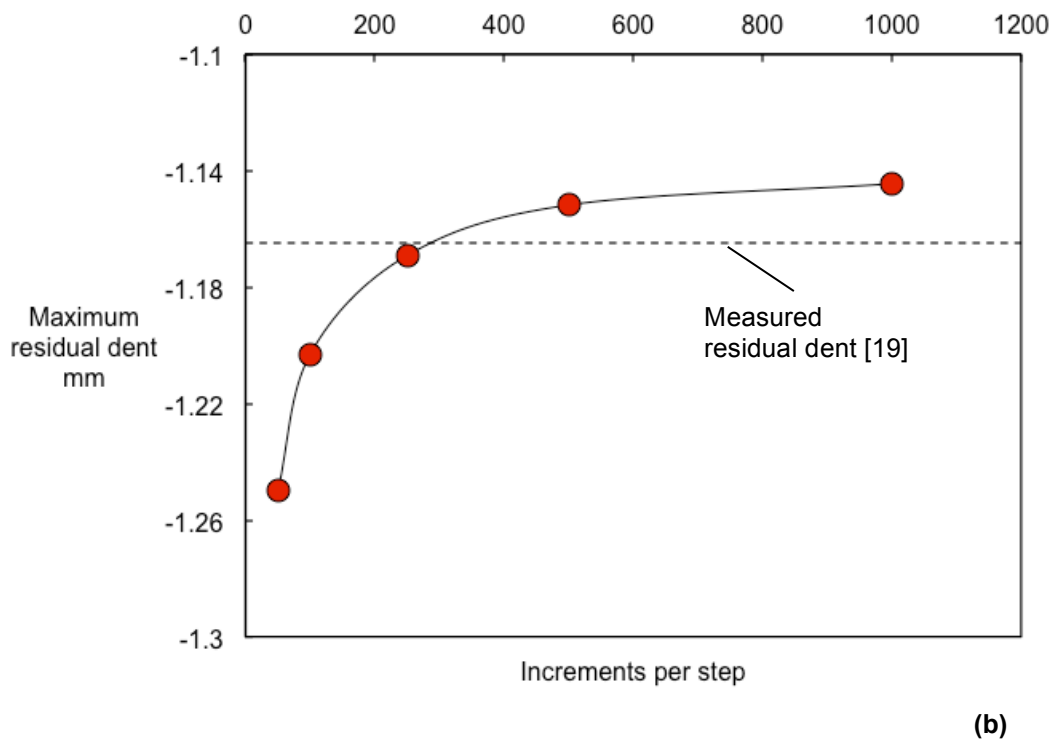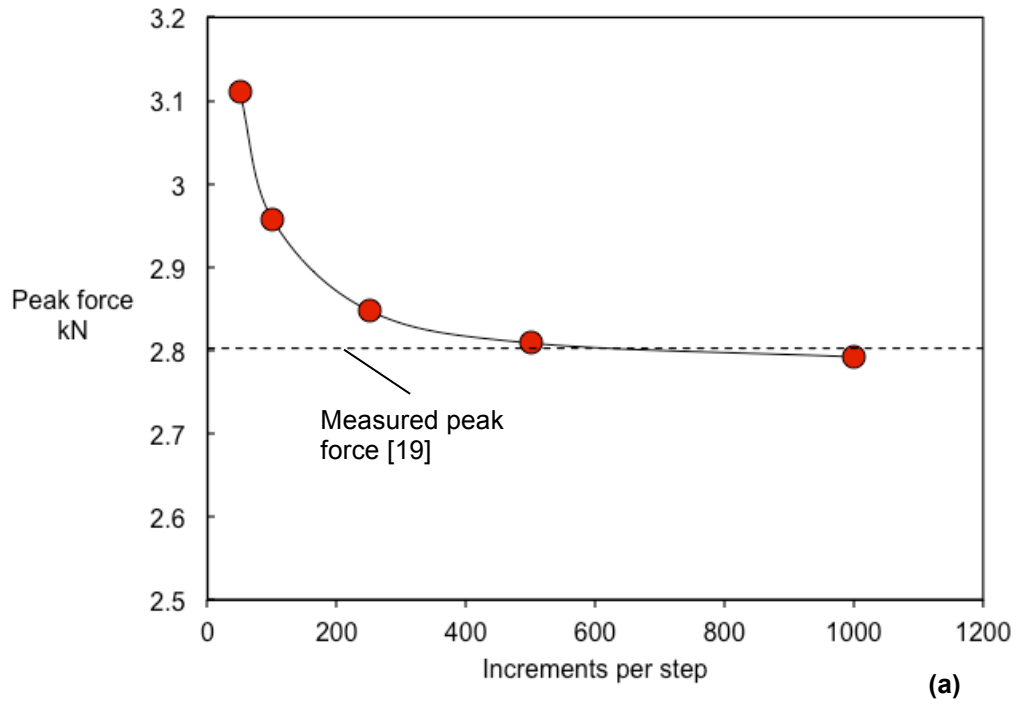Figure 7. Computed versus measured residual indentation depths in QSI specimens.

Figure 8. (a) Computed peak force versus increments per step, (b) Computed maximum resicual dent versus increments per step.

TABLE I. MATERIAL PROPERTIES USED IN ANALYSES.

Facesheet ply properties [20]		
E_{11}= 143.0 GPa	E_{22} = 12.9 GPa	E_{33} = 11.7 GPa
ν_{12} = 0.32	ν_{13} = 0.32	ν_{23} = 0.44
G_{12} = 4.1 GPa	G_{13} = 4.1 GPa	G_{23} = 3.98 GPa
UMAT input (Figure 3) [20]		
σ_b=2MPa	σ_c=0.84MPa	σ_{cc}=1.12MPa
σ_{tt}=0.01MPa	σ_t=1MPa	k=1.26
e_1=1180$\mu\varepsilon$	e_2=10660$\mu\varepsilon$	e_3=98800$\mu\varepsilon$

TABLE II. COMPUTED AND MEASURED QSI SPECIMEN RESPONSE.

25mm indentor QSI test			
	Computed	Measured [20]	% difference
Peak force (kN)	1310	1300	<1%
Max residual dent (mm)	0.48	0.59	-19%
Total energy dissipation (Nmm)	632	701	-9.8%
76mm indentor QSI test			
	Computed	Measured [20]	% difference
Peak force (kN)	2790	2800	<1%
Max residual dent (mm)	1.09	1.16	-6%
Total energy dissipation (Nmm)	2340	2599	-9.9%